Flocculation of Colloids Suspended in a Viscoelastic Fluid Undergoing Shear

The effect of viscoelasticity on the kinetics of the shear-induced flocculation of colloids has been investigated theoretically and experimentally. A numerical technique for such three-dimensional problems called global residual minimization (GRM) has been developed as an alternative to finite element and finite difference methods. In the GRM method, minimization of the residual of the momentum balance is used as the selection criterion for the velocity-field solution. Trajectory simulations were carried out for spheres in a corotational Jeffreys fluid at a variety of Weissenberg numbers, *We*. For $We \leq 0.01$, the effect of viscoelasticity is found to be negligible. For $We = 1.0$, flocculation rates are enhanced. For $We = 10.0$, a possibly large reduction in flocculation rate is indicated.

Experiments were conducted using 600 nm radius polystyrene spheres in hydroxyethyl cellulose solutions. At shear rates corresponding roughly to $We = 10.5$ and 15.3, the flocculation rates were found to be at least an order of magnitude less than the rate expected in a Newtonian fluid. It is postulated that this reduction in flocculation rate is caused by the viscoelasticity of the suspending fluid.

R. T. Mifflin, W. R. Schowalter
Department of Chemical Engineering
Princeton University
Princeton, NJ 08544

Introduction

Many colloidal suspensions, ranging from biological fluids and foodstuffs to paints and pharmaceuticals, contain dissolved polymer in the continuous phase. The presence of this polymer can be only incidental to the behavior of the suspension or it can exert great influence, even in small quantities. Although steric and thermodynamic effects often dominate the behavior of the suspension (Napper, 1983), hydrodynamic influences can also be important. This is particularly evident when the polymer acts as a thickener. At very high concentrations the polymer may even form a gel-like structure around the dispersed phase; however, we consider here only the case in which the suspending material is most accurately described as a fluid, rather than as a solid.

Even qualitative results on the hydrodynamic effects of polymer solutions are lacking. This is mainly due to two factors: the nonlinear rheology of polymer solutions, and the difficulty of isolating hydrodynamic from thermodynamic and steric effects. In this study, we take a first step toward elucidating the viscoelastic influence. The theoretical work presented in this paper includes only hydrodynamic forces, and in the experimental work we have attempted to match the conditions of the theory. Thus, we do not at present consider the interplay of the hydrodynamics with the various other effects, which may well be important in practical situations.

Of course, one must also consider the forces between colloidal particles that occur even in the absence of polymer. These forces are electrostatic repulsion, van der Waals attraction, Brownian forces, and solvent-structure or hydration forces. Reviews of these forces and their significance are available in the literature (Mahanty and Ninham, 1976; Hunter, 1981; Russel, 1981; Israelachvili, 1985). It will be shown that all of these effects can be made negligible, except for the van der Waals attraction, which is critical to the measurements we shall report. It is the strength of the van der Waals force that is used as a yardstick by which the magnitude of the hydrodynamic forces is determined.

We compare van der Waals and hydrodynamic forces by studying flocculation kinetics. In flocculation kinetics studies, uniform suspensions of monodisperse colloidal particles are sheared for given amounts of time. During the initial stage of the process, single particles coagulate into doublets. A count of the

R. T. Mifflin is currently with Exxon Production Research Co., Houston, TX 77252-2189.

doublets formed over various times after initiation of shear provides a scalar measure of the relative magnitude of the van der Waals attraction that brings particles together and the hydrodynamic forces that tend to sweep the particles past one another in the very low Reynolds number flows commonly encountered in colloidal suspensions.

Examples of flocculation kinetics studies for colloidal particles in Newtonian fluids under shear have been presented by van de Ven and Mason (1976) and Zeichner and Schowalter (1979). Feke and Schowalter (1983) give an improved estimate for the initial flocculation rate in laminar shear. From their Figure 13 one can approximate the initial flocculation rate in laminar shear flow by

$$J_{Sh} = 6.5(Fl)^{-0.23}a^3\dot{\gamma}n_0^2 \qquad (1)$$

where J_{Sh} is the rate of disappearance of singlets per unit volume of suspension, a is the particle radius, $\dot{\gamma}$ is the shear rate, n_0 is the initial number density of singlets, and $Fl = 6\pi\mu a^3\dot{\gamma}/A$ is the flow number, μ being the viscosity and A the Hamaker constant, a measure of the strength of the van der Waals attractive forces. (Note that J_{Sh} differs by a factor of 2 from the collision rate with a test sphere used by Feke and Schowalter, 1983.)

A naive attempt to account for the hydrodynamic effects of the solution polymer is to use an effective viscosity; that is, to assume that the polymer solution behaves as a Newtonian fluid with a viscosity equal to the viscometric function $\mu(\dot{\gamma})$ evaluated at some characteristic shear rate. Because of the weak dependence shown in Eq. 1 of J_{Sh} on viscosity, the choice of characteristic shear rate at which the viscosity is evaluated is unimportant except for cases in which the solution is highly shear thinning over the range of shear rates of interest. There is reason to believe that this naive approach will be inaccurate, in that the flocculation rate will depend very critically on the behavior of the fluid in the gap region between the spheres as they come together in the shearing field, Figure 1. In this region shear thinning may reduce the resistance to flocculation, but a high extensional viscosity may brace the spheres apart until the shearing field sweeps them past one another. Thus one can reason that there are competing effects that can lead to either increases or decreases in flocculation rates.

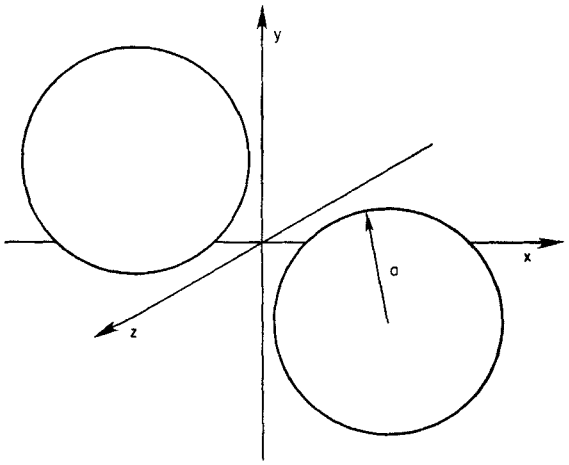

Figure 1. Two-sphere geometry.
Sphere centers are in the plane $z = 0$; imposed velocity field is $v = \dot{\gamma}yi_x$

To estimate the magnitude of these effects, consider the trajectories of particles in a Newtonian fluid, Figure 2. Note that a large upstream region contributes trajectories that result in the spheres coming quite close together. Imagine the locus of the limiting orbiting trajectory being changed so that the spheres can come no closer than 0.1 particle radius. Now, even at low shear rates, very few particles will reach sufficiently small separations for van der Waals forces to cause aggregation. Alternatively, consider the high shear rate case, in which the upstream region of flocculating trajectories is reduced even further because now the spheres must come even closer for van der Waals forces to overcome the hydrodynamic forces. A reduction of the effective viscosity in the gap would allow smaller separations, and the upstream region of flocculating trajectories could grow significantly in relation to the Newtonian case. Thus, it can be seen that a change in the characteristic viscosity inside the gap by a factor of 2 or 3 from the value outside the gap can have a substantial effect on the flocculation rate. It is the purpose of this study to determine from theory and experiment whether such dramatic effects do indeed exist.

Theory

Purpose and general description

We wish to determine whether, in a qualitative sense, the hydrodynamic effect of added polymer will enhance, retard, or have no effect on the rate of flocculation under shear. Although van der Waals attractive forces can, in principle, be incorporated into our calculations, we prefer to begin with the simpler problem in which only forces of hydrodynamic origin are included. This corresponds to the limiting case of flow number $Fl = \infty$. Because in practice the Reynolds number, defined by $Re = \rho\dot{\gamma}a^2/\mu$, where ρ is the fluid density, is below 10^{-3}, we have neglected inertia.

The only result to date for a three-dimensional shear flow problem with spheres suspended in a rheologically complex fluid has been Peery's (1966) solution for a single sphere in a second-order fluid. Some solutions have been determined as part of the work described here for single spheres in finitely viscoelastic

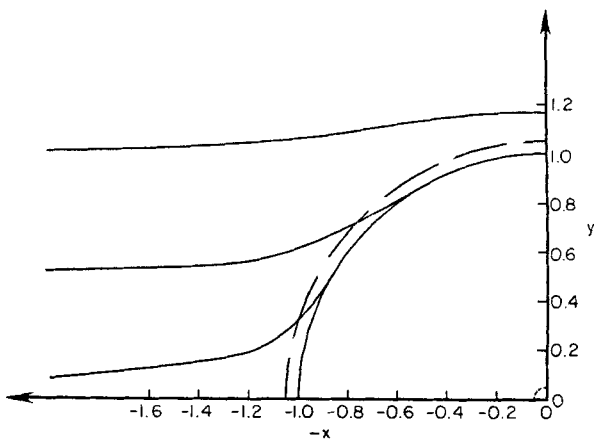

Figure 2. Newtonian particle trajectories.
Trajectory with smallest y values is the limit of the orbiting trajectories
——— Surface at which particle separation reaches 0.1 particle radius; this might be called a "flocculation surface," although the exact point at which the van der Waals attraction begins to dominate depends on the flow strength

fluids (Mifflin, 1986; Mifflin and Schowalter, 1986). Apart from these, however, only Bush et al. (1984) have solved a three-dimensional flow for a viscoelastic fluid. Their technique, which appears promising, involves iteration between boundary elements and interior elements. However, an initial guess for the stress field is required, and the iterations may not converge.

One might expect that it would be possible to apply the results for the approach of two flat plates to the problem of approaching spheres. However, with a non-Newtonian fluid there is at best a tenuous connection between the sphere-sphere problem and the plate-plate problem. The deceleration of the fluid as it is squeezed out of the gap and the rotation of the spheres destroy a useful analogy for nonlinear fluids.

Thus we are forced to work with the full geometry shown in Figure 1. It is clear that inversion symmetry exists through the origin. We further symmetrize the problem by considering only sphere centers that are in the plane $z = 0$, so that there is reflection symmetry in the xy plane. The consequences of this restriction are noted in the discussion of theoretical results.

Boundary conditions include the requirement of no relative motion at the sphere surface. Thus

$$v = v_\alpha + \omega_\alpha i_z \times (r - r_\alpha); \quad \alpha = 1, 2 \tag{2}$$

for r on the surface of a sphere α. The sphere centers are at r_α, and their velocities are v_α. Symmetry requirements force the relations

$$v_1 = -v_2, \quad v_1 \cdot i_z = 0$$
$$\omega_1 = \omega_2 = \omega, \quad r_1 = -r_2 \tag{3}$$

At large distances from the spheres we require that the flow field approach that of simple shear

$$v \to E \cdot r \quad \text{as } |r| \to \infty \tag{4}$$

We deal only with incompressible fluids. Thus the continuity equation is $\nabla \cdot v = 0$, and because inertia is assumed to be negligible, the momentum balance is $\nabla p = \nabla \cdot T$.

To complete the problem specification one must specify the stress T as a function of the deformation history. We use the corotational Jeffreys model (Bird et al., 1977, p. 327ff) in integral form, although the technique to be described can be used with almost any integral constitutive relation. The corotational Jeffreys model is particularly convenient because evaluation of the memory integral, which requires tracking of fluid elements backward in time, is easier than it would be if a codeformational model were used. Computer time in excess of that available would be required to determine whether the limitations of the Jeffreys model are important in a qualitative sense. It is our conjecture that they are not. The extra stress is given by

$$T = 2\int_{-\infty}^{t} \{(1 - \beta)/We \exp[(t' - t)/We] + \beta\delta(t)\} L(t, t')dt' \tag{7}$$

where

$$L(t, t') = R(t, t') \cdot G(t') \cdot R^T(t, t')$$

with

$$G(t') = [(\nabla v + (\nabla v)^T]/2$$

Superscript T indicates transpose.
$R(t, t')$, the rotation tensor, is defined by

$$\partial R(t, t')/\partial t' = R(t, t') \cdot W(t'), \quad R(t, t) = I \tag{8}$$

where

$$W(t) = [(\nabla v) - (\nabla v)^T]/2.$$

Note that ∇v here is defined such that its physical components are given by $(\nabla v)_{ij} = \partial v_j/\partial x_i$.

The Weissenberg number, We, is equal to $\lambda_1\dot{\gamma}$, where λ_1 is the relaxation time. We have written β for the ratio λ_2/λ_1, in which λ_2 is called the retardation time. Time is scaled on the reciprocal shear rate, lengths are scaled on the particle radius, and velocities are scaled on the product of particle radius and shear rate. The stress is scaled on $\mu_0\dot{\gamma}$, where μ_0 is the viscosity at zero shear rate.

Before attempting to solve the problem it is worthwhile to consider the kinds of behavior one might expect. In general, it seems unlikely that the fluid outside the gap region will alter its course greatly with respect to the flow of a Newtonian fluid unless We is very large. Observations of numerical solutions of flows with finite viscoelasticity have shown that the velocity field in the non-Newtonian case is often very similar to the Newtonian velocity field (Tiefenbruck and Leal, 1982). However, as the spheres come together, it might be expected that the extensional nature of the flow in the gap could cause "channeling." Here channeling refers to a phenomenon best considered in terms of the flow in a sudden contraction (Schowalter, 1978, p. 219). The flow undergoes a drastic rearrangement in response to the extensional, accelerated nature of the contraction flow. We therefore seek flow rearrangements in the gap between the spheres, and we try to assess the impact of such rearrangement on the flocculation rate under shear.

Global residual minimization method

When one attempts to construct a flow field using finite elements, each degree of freedom, or appropriately weighted basis function, corresponds to a small, localized flow. The sum of these flows then gives a detailed picture of the overall field. In global residual minimization (GRM), each degree of freedom is a global flow field representing some characteristic of the overall flow. If these global flow fields are properly selected, the general behavior of so-called secondary flows is economically reflected in a few degrees of freedom.

The use of the GRM method to calculate secondary flows has been described earlier (Mifflin and Schowalter, 1986). The calculation was for the steady-state problem of a single sphere in a shear flow, but many of the ideas transfer directly to the present problem. Below, all the steps of the method will be presented, but only those features specific to the two-sphere flocculation problem will be emphasized. Complete details on both problems are available elsewhere (Mifflin, 1986).

We are primarily interested in the behavior when the two spheres are close together. Also, we expect that hydrodynamic interactions will be dominated by flow in the gap between the

spheres. Therefore, we model the flow in the gap using the GRM technique. Using the stress fields thus generated, one can construct trajectories for the sphere centers and chart the influence of hydrodynamics on a flocculation encounter. The steps in this process are outlined below.

Basis functions

In the GRM method, the velocity field is represented as a sum of basis functions, $v_i(x)$:

$$v(x) = \sum_i c_i v_i(x) \tag{9}$$

Each basis field is solenoidal, so that incompressibility is satisfied identically for any choice of coefficients. For a two-sphere geometry, bipolar spherical coordinates are a natural choice for representing these fields. However, we are primarily interested in major changes in the sphere-sphere interaction hydrodynamics, and we therefore concentrate on the gap region between the spheres.

In the gap it is convenient to use lubrication coordinates (Cox, 1974), which are stretched cylindrical coordinates. We then construct solenoidal basis fields using the technique of poloidal and toroidal fields (Chandrasekhar, 1961, p. 225). We impose the symmetry constraints and require that the velocity-field derivatives remain bounded everywhere and that the velocity perturbation to Eq. 4 approach zero outside the gap.

The primary flow is taken as the flow of a Newtonian fluid based on the sphere motions and rotations. This flow clearly satisfies the symmetry and incompressibility constraints. The effect of viscoelasticity is to impose a secondary flow on this primary solution. As the Newtonian flow satisfies the boundary conditions on the sphere, all other basis functions must have zero velocity on the sphere surfaces.

To model the secondary flow we have used the simplest toroidal field and the simplest poloidal field that satisfy the constraints. The poloidal field, shown in Figure 3, is axisymmetric about the sphere-sphere axis. The toroidal field is more difficult to represent, but the streamlines and velocity fields in one plane are given in Figure 4. The x and y are laboratory coordinates, and the r and z are sphere-sphere cylindrical coordinates. Expressions for these fields are given in the appendix.

Stress field

For any given set of basis function coefficients, we can explicitly construct the extra stress field by integrating the constitutive relation along a streamline back in time from the present. Clearly, any constitutive relation that can be integrated explicitly could be used here. Details of the integration are given elsewhere (Mifflin, 1986).

To reduce the cost of determining the basis function coefficients, a macrostep/microstep method has been developed for the time steps. Each macrostep was divided into 10 microsteps. With each microstep the spheres move, and the sphere-sphere axis rotates with respect to the laboratory system, but the coefficients of the poloidal and toroidal fields are held fixed over a macrostep. Thus, the basis function coefficient determination is required only once per macrostep. Another economy was employed for calculation of the stress field. In order to calculate the stress in the gap, one incorporates the velocity gradient history of fluid elements in the gap. To calculate the effect of history of those elements prior to entry into the gap region, the kinematics of Eq. 4 were used. Similarly, when the stepping back in time reaches the beginning of the simulation, Eq. 4 is invoked for all earlier times.

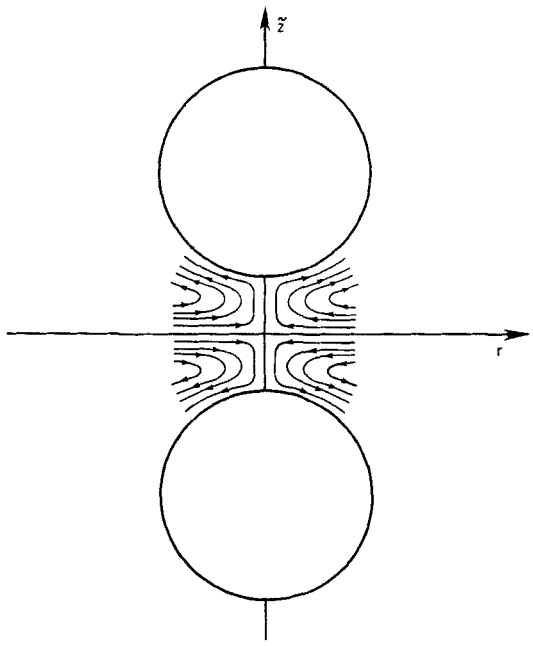

Figure 3. Poloidal field: streamlines representing poloidal basis function for the two-sphere problem.
r, $\tilde{z}$, Cylindrical coordinate system with respect to sphere-sphere axis

In order to obtain forces on the spheres, one requires the pressure on the sphere surfaces. The reference pressure was set equal to zero at infinity and the momentum balance was then inte-

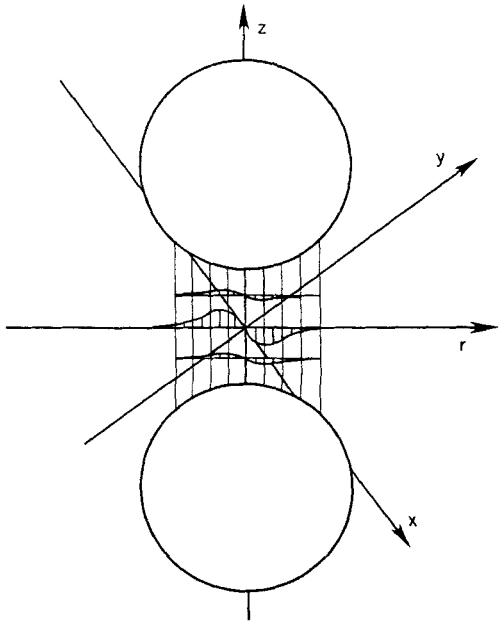

Figure 4. Toroidal field.
Velocity vectors and streamlines in xy plane in laboratory-frame coordinates, which is also $\phi = 0$ plane in sphere-sphere cylindrical coordinates

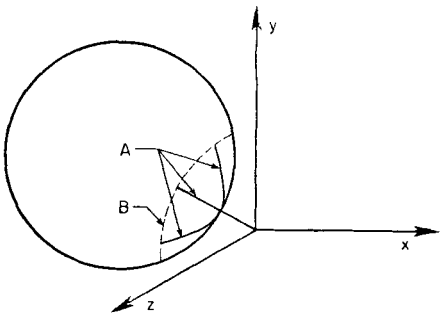

Figure 5. Surface integration paths. Integration paths *A* indicated for surface calculations; — — — curve *B* denotes arbitrary edge of gap region

grated along the z axis of the laboratory frame, Figure 1, to the origin and then along the sphere-sphere axis to the point of closest approach of the spheres. The momentum balance integrated along the paths A of Figure 5 then gives the pressure along those curves. This was done throughout the gap region. (See the appendix for a definition of the gap region.)

The extra stress at any point on the sphere is obtained by siting a streamline at that point and integrating the constitutive relation back in time from there. Adding in the pressure then provides total stress. The gap faces of the spheres were divided into several regions. The stress was evaluated at the center of each region and approximated as a constant over the region. The force and torque on the sphere due to stresses in the gap were then obtained by summation.

Outside of the gap region an estimate of the stress and pressure on the sphere was employed. The stress was taken to be that which would result if the fluid were Newtonian but possessed a viscosity corresponding to that of the suspending fluid undergoing simple shear at a rate of deformation corresponding to $\boldsymbol{E}$ of Eq. 4 (Mifflin, 1986).

Iterations on particle motions

For any given set of basis function coefficients of the poloidal and toroidal fields, there is a set of sphere motions such that the force and torque are zero. We use a numerical-Jacobian Newton-Raphson procedure to determine the motions. The changes in force and torque are calculated for small changes in each of the three independent particle motions. Numerical differentiation gives the Jacobian, which is inverted to determine the next guess for the particle velocities and rotation rates.

Iteration on basis function coordinates—the residual calculation

Once the particle motions are determined, all of the governing equations are satisfied except the momentum balance in the fluid. Taking the curl of this equation gives

$$\nabla \times \nabla \cdot \boldsymbol{T} = \boldsymbol{0} \tag{10}$$

We treat the magnitude of the curl of the divergence of the extra stress as a measure of the error in the momentum balance:

$$q = |\nabla \times \nabla \cdot \boldsymbol{T}| \tag{11}$$

where q is called the residual. Basis function coefficients are chosen to minimize a sum of q^2 at selected points within the gap region. The residual q is calculated using a bundle of 27 streamlines centered about one of the selected points. Using the stress at these 27 points, we calculate a smoothed version of the second derivative of the extra stress, thus obtaining q. Details are given by Mifflin (1986) and Mifflin and Schowalter (1986).

To determine an optimum choice of basis function coefficients, one steps along a grid of values of the coefficients until a set of coefficients is reached such that all neighboring sets give larger residuals. This completes the execution of a time step. One then proceeds to the next macrostep using the coefficients of the previous step as the initial guess.

Results and Discussion of Calculations

Parameter settings

Trajectories have been calculated for $We = 0.1$, 1.0, and 10.0. In each case we have set $\beta = 0.2$. We show only the coordinates of one of the sphere centers (x, y); the other sphere center is at $(-x, -y)$. The coordinate system is shown in Figure 6. Sphere-sphere contact occurs when $x^2 + y^2 = 1$, depicted as a solid circular arc in Figure 6. Calculations of the trajectories are started at a surface-to-surface separation of about one sphere radius. This separation was sufficient to ensure that the results were only weakly dependent on the exact location of initiation of the trajectory calculation. Representative trajectories are initiated at three locations, whose (x, y) coordinates are $(-1.3, 0.7)$, $(-1.5, 0.5)$, and $(-1.5, 0.3)$. These trajectories are labeled A, B, and C, respectively. They span the range relevant to flocculation at moderate flow numbers, that is, $Fl < 0(10^3)$.

The sizes of time steps were chosen to be the largest possible without significantly altering the sphere paths. With five microsteps per macrostep, the microstep sizes varied from 0.016 to 0.06. For each run, the time step was held constant.

In all of the simulations, momentum balance residuals were calculated at 10 points dispersed evenly throughout the symmetry element of the gap region. The exact placement of these residual calculation points was found not to be crucial.

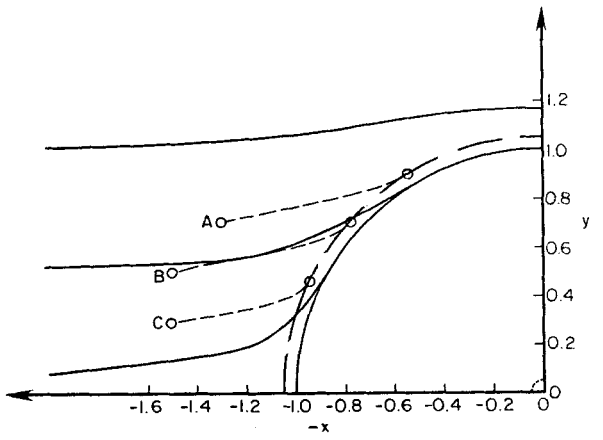

Figure 6. Newtonian trajectories calculated by GRM method for *We* = 0.0.

Trajectories *A*, *B*, *C* terminate at a 0.1 dimensionless separation, large ——— curve

—— True Newtonian trajectories

Small --- curve at origin indicates locus of points of closest approach of sphere surfaces when large — — curve is reached by sphere centers

We require that the basis function coefficients lie on a grid of discrete values. With the basis functions themselves scaled to have a maximum velocity of 0(1), a useful grid size was found to be 0.02 for field 1 (the poloidal field) and 0.01 for field 2 (the toroidal field).

Results

The first test of the method is to set $We = 0.0$ and to check calculated trajectories against known solutions for a Newtonian fluid. A comparison is shown in Figure 6, where the solid lines are three representative Newtonian trajectories. *A*, *B*, and *C* are the trajectories calculated for $We = 0.0$. These will be termed "calculated Newtonian" trajectories.

Because van der Waals forces have not been included in our calculations, an exact calculation of particle-particle separation below which flocculation occurs is not possible. As a first estimate we chose a sphere-sphere separation of 0.1 and stopped our calculations when this separation was reached. This value was dictated in part by the fact that trajectory calculations became rapidly more difficult as separations were reduced below 0.1. The choice is based on an expectation that van der Waals attraction will dominate at separations smaller than 0.1. The actual interparticle separation will of course depend on ionic strength and other parameters, but the computational cost of a more detailed study did not seem justified.

When comparing the calculated Newtonian trajectories with the true Newtonian trajectories in Figure 6, it is important to recognize that true Newonian trajectories fill the entire space outside of $x^2 + y^2 = 1$. Approximate trajectories can be constructed by interpolation from those shown. In each comparison, the proper criterion for accuracy of a calculated Newtonian trajectory is the degree to which the slope of the trajectory matches that of the true Newtonian path at the same point in space. The inability of the calculated Newtonian trajectories to match the true Newtonian slope everywhere is an indication of the effects of the various approximations made in the calculation process.

Trajectories for $We = 0.1$ are shown in Figure 7. For $We = 0.001$ and $We = 0.01$, the particle paths are indistinguishable from the calculated Newtonian trajectories. The $We = 0.1$ trajectories bring the spheres somewhat closer together relative to the calculated Newtonian trajectories, but it is not clear that the difference from Figure 6 is significant.

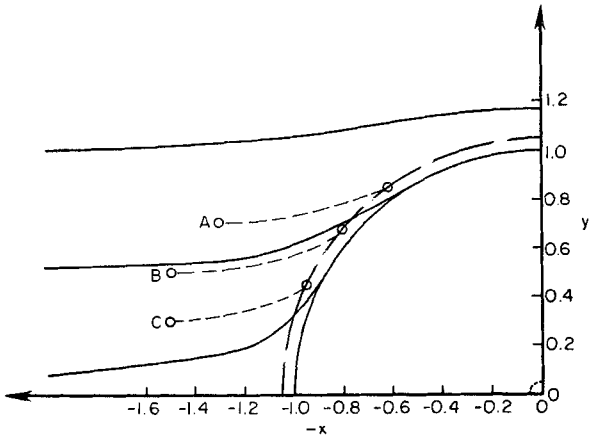

Figure 7. Trajectories calculated by GRM method for $We = 0.1$.
A, *B*, and *C* terminate as in Figure 6

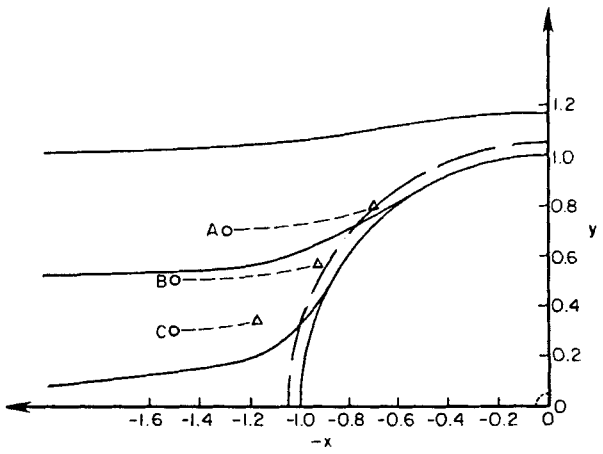

Figure 8. Trajectories calculated by GRM method for $We = 1.0$.
A, *B*, *C* terminate as in Figure 6
Δ abnormal terminations of trajectory calculations

The trajectories for $We = 1.0$ are shown in Figure 8. These particle paths indicate less net hydrodynamic resistance than those at $We = 0.1$. The triangles at the downstream ends of the trajectories indicate that the basis function coefficient search failed to converge. This is perhaps indicative of a large change in flow field that cannot be tolerated by the program unless the step sizes are reduced.

The trajectories for $We = 10.0$ are shown in Figure 9. The particle paths have moved in such a way that particles remain farther apart, indicating greater hydrodynamic resistance. Again, the basis function coefficient search failed to converge at the points indicated by triangles in the figure.

Discussion

One normally considers the effects of viscoelasticity in terms of the viscometric functions, these being measures of shear thinning and of normal stress differences. Shear thinning will result

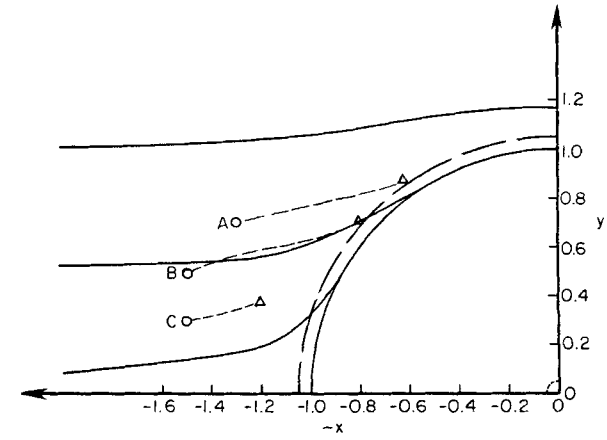

Figure 9. Trajectories calculated by GRM method for $We = 10.0$.
A, *B*, *C* terminate as in Figure 6.
Δ abnormal terminations of trajectory calculations

in less hydrodynamic resistance, as the gap region tends to have a higher shear rate than the external flow. Elastic effects will tend to keep the spheres apart. (Juxtaposition of effects of shear thinning and elasticity provides, we believe, a convenient and meaningful physical picture. However, it is possible to have materials, such as fiber suspensions, for which a high extensional viscosity is not due to elasticity.) In the results just shown, shear thinning appears to dominate at $We = 1.0$, while elastic effects dominate at $We = 10.0$. The latter result is not unexpected, considering that the shear thinning properties of the corotational Jeffreys fluid are expected to saturate at $We = 0(10)$. It would be of interest to use constitutive relations that displayed shear thinning over a greater range of We. Also, unsteady responses of the fluid can be important in this type of flow. Further characterization of the fluid in this regard would be useful.

We next use the trajectory results to make inferences about flocculation rates. Of course, the magnitude of fluid stresses due to hydrodynamics relative to the van der Waals attraction will be critical. The flocculation rate will be determined by the area of upstream trajectories that result in aggregation and the velocity at which particles travel along those trajectories. It is clear that if the hydrodynamics causes the trajectories to "kick out" and avoid close approach of the spheres, the van der Waals attraction cannot drag many of the particles across the hydrodynamic trajectories and cause flocculation, except when the attraction is large with respect to the hydrodynamic forces. In order for these viscoelastic effects to be pronounced, we must have a large ratio of hydrodynamic to van der Waals forces.

At $We = 1.0$ flocculation rates will be somewhat enhanced but probably not more than approximately a factor of 4 for $Fl < 0(10^4)$, because the upstream area of trajectories that result in flocculation has expanded by at most a factor of about 2. At $We = 10.0$, we would predict a decrease in flocculation rates, but here we would expect a more dramatic effect, particularly at high ratios of the hydrodynamic force to the van der Waals force. Without a continuation of the trajectories to smaller separations, it is not possible to make a quantitative estimate of the extent of the reduction in the rate of aggregation, but it would appear that if van der Waals forces are sufficiently weak [$Fl > 0(10^3)$] the reduction could be several orders of magnitude. Particle encounters for which the sphere centers are not in the plane $z = 0$ will of course be different in detail. However, they are not expected to alter the overall flocculation rate in a manner qualitatively different from that found in the plane $z = 0$. The additional efforts needed in order to include such trajectories are described in Mifflin (1986).

Experimental Method

Purpose and background

The purpose of the experimental portion of this work is to determine the effects of the viscoelasticity of the suspending medium on colloidal flocculation. To correspond with the theoretical analysis, we seek conditions under which large changes in rates of flocculation are possible. Hence solution concentrations are accurate only to within a few percent, except where indicated, and we have not carried out the large number of runs necessary for a useful statistical analysis. There are, however, some qualitative aspects that must be carefully considered. First, we try to isolate the effects of hydrodynamics by eliminating all other effects except van der Waals attraction. Thus we seek to render negligible the electrostatic repulsions, solvent structure forces, Brownian motion of the particles, effects due to polymer-solution inhomogeneity, and specific interactions between polymer and particles.

The flocculation experiments of Feke and Schowalter (1985) bear much in common with the present experiments. The particles were synthesized in essentially the same way, and the same Couette shear apparatus was used in both sets of experiments. Also, both researches were concerned only with the formation of doublets from singlets, that is, the initial flocculation rate. In the Feke and Schowalter experiments, however, the effect of weak Brownian motion in shear-induced flocculation was studied. We use their estimated effective Hamaker constant, A, of 5×10^{-21} J for polystyrene latices. We also use their theoretical results (Feke and Schowalter, 1983) for flocculation rates in Newtonian fluids as a basis for comparison with the present results.

Materials

Particles. Polystyrene latex particles were synthesized following the surfactant-free emulsion polymerization described by Goodwin et al. (1976). The particles were cleaned by repeated centrifugation and resuspension in deionized water and were sized by transmission electron microscopy. Over 30 measurements gave a mean diameter of 1.2 μm, with a range of ± 50 nm covering all the particles measured but one. Volume fraction was determined by drying and weighing by difference. Using the known densities of water and of polystyrene (1.057 g/mL), the volume fraction of particles was found to be 0.063. The exact electrical properties of the particles are not critical to the investigation conducted here; the zeta potential is estimated to be about 70 mV in 0.1 M KCl.

To determine the state of aggregation of the particles, we use particle counting. The instrument used was an Elzone Electrozone particle sizer made by Particle Data, Inc. Tests were conducted to ensure that no appreciable flocculation was caused by the measurement process. Repeptization was found to occur only for flocs of the order of 10 particles or larger. Particle analysis indicated that approximately 10% of the particles synthesized were initially in the form of doublets; this presence of doublets was factored in for each of the experiments.

Polymer. We sought a polymer solution that matched the viscometric characteristics of a Jeffreys fluid with a viscosity ratio, μ_∞/μ_0 ($\equiv\beta$), of 0.2, as used in the theoretical analysis. Also required was a polymer that would not strongly adsorb to the polystyrene particles. The nonadsorbing polymer system employed by Sperry et al. (1981)—polystyrene particles and hydroxyethyl cellulose (HEC) as a solution polymer—was used. Sperry et al. found that Triton X-405 surfactant acted to displace any adsorbed HEC. We replaced Triton X-405 with Triton X-100 in order to reduce the size of the surfactant layer on the particles.

It is possible for cellulosic polymers to form microcrystals (Battista, 1975). However, in our case even the largest microcrystals would be much smaller than the 1.2 μm particles and therefore unlikely to disturb the continuum hypothesis for the suspending medium. Nevertheless, at the high salt concentrations used here these microcrystals can aggregate just as colloidal particles and interfere with the particle size distribution analysis. These aggregates do not pose a problem during the

flocculation processes because any microcrystals will be immersed in a background of polymer and will merely represent a somewhat higher than average local concentration of polymer.

In order to eliminate microcrystalline aggregates, we mixed samples with 1.0 M HCl for 20 h before performing particle aggregate distribution analyses. The particles themselves have highly acidic sulfate surface groups and were not affected by the process. All samples were neutralized prior to particle analysis.

The HEC was supplied by Hercules, Inc., in two viscosity-average molecular weights: 225,000 (called GR) and 613,000 (called MR). Information on these polymers is available from Hercules and from Sperry et al. (1981). Each prepared polymer solution contained 1.2 M NaCl, 2 g/L Triton X-100, and 0.2 g/L NaN_3. The NaN_3 is an antibacterial agent. The concentration of NaCl used ensures that after mixing with an equal volume of effectively salt-free suspension, the double layers of the particles will be small enough to have no effect on the flocculation process. The high salt concentration also helps to render the solvent structuring negligible for particle separations greater than the width of a few water molecules.

Particle contaminants were removed from the polymer solutions via ultracentrifugation at an average g force of 23,000 for 1 h. A small amount of the polymer (no more than 5 wt. %) was lost in the process, resulting in solutions with smaller concentrations than nominally given. Rheological properties of the polymer solutions were determined on a Rheometrics System IV rheometer. Viscosities and primary normal stress differences of the polymer solutions were measured at shear rates up to 500 s^{-1}. Various concentrations were prepared and tested to find the best fit to the rheological model used in the theory. For the GR polymer, 40 g/L gave the best fit, and 12.5 g/L gave the best fit for the MR polymer. Rheological data are shown in Figure 10. It is clear that the Jeffreys model provides a consistent match of shear and normal stress data over the mid-range shear rates but is not always satisfactory at the extremes.

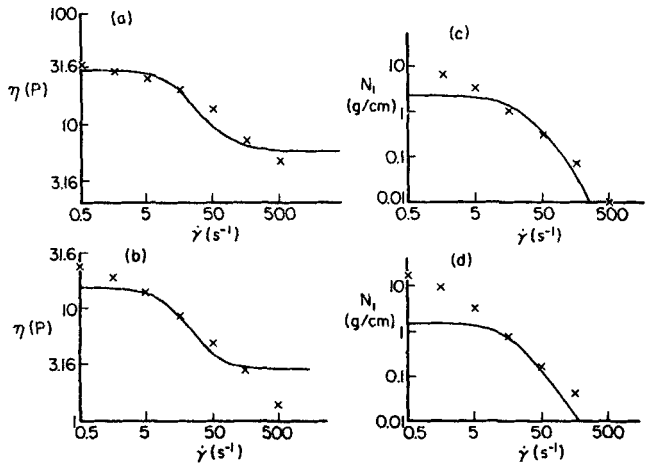

Figure 10. Viscosities and normal stresses.

Fitted and measured viscosities μ and primary normal stress differences N_1 as functions of shear rate

X measurements made with cone and plate, steady setting of rheometer; cone angle = 0.04 rad

——— behavior of corotational Jeffreys model using parameters chosen to fit viscosity data

(a), (c) 40 g/L GR HEC; relaxation time λ_1 = 0.05 s; retardation/relaxation ratio β = 0.2; zero shear rate viscosity μ_0 = 30 poise

(b), (d) 12.5 g/L MR HEC; relaxation time λ_1 = 0.067 s; retardation/relaxation ratio β = 0.2; zero shear rate viscosity μ_0 = 15 poise

No adjustable parameters were used to fit $N_1/\dot{\gamma}^2$

As mentioned before, the polymer was mixed with an equal volume of the latex suspension. Thus, solutions were prepared at 80 g/L of GR polymer and 25 g/L of MR polymer.

To treat the polymer as a homogeneous medium, one must ensure that the polymer chains are overlapped. This was tested by considering the zero shear rate viscosity as a function of molecular weight (Graessley, 1974). We found the zero shear rate viscosity to be approximately proportional to molecular weight to the 3.4 power, thus indicating entanglement.

Other Materials. Other materials were salt, acid, base, and surfactant solutions. Dust particles were removed using 0.22 μm Millipore filters. A single filtration was found to be quite effective for removing extraneous particles.

Experimental Procedures and Results

Before describing the procedures and results, we provide an overview of the experiments that were needed to determine the effect of viscoelasticity on the flocculation process. We first tested surfactant-coated particles in Brownian flocculation in water to make sure that the particles were not permanently stabilized by the surfactant layer. Then the flocculation behavior of the particles with surfactant in water under shear was checked, because hydrodynamic effects of the adsorbed layer could be somewhat different under shear than under Brownian coagulation. Finally, the particles were flocculated in polymer under shear, and the aggregation rate was compared with that expected in a Newtonian solution.

Brownian flocculation in water

For the experiment of Brownian flocculation in water, a suspension of particles at a volume fraction of 3.6×10^{-4} was mixed with an equal volume of 1.2 M NaCl. Samples were taken after 0, 5, 10, 20, and 30 min, and each was immediately diluted to halt the flocculation process.

From the particle counter, the fraction of singlets, f, as a function of time, t, was determined. The theory of Brownian flocculation predicts that $f(\tau) = 1/(1 + \tau)^2$, where $\tau = 4kTn_0t/3\mu W_{Br}$ (Feke and Schowalter, 1985). Here, k is Boltzmann's constant, T is the temperature, n_0 is the initial number concentration of particles, and W_{Br} is a factor called the Brownian stability ratio. Thus, from the plot in Figure 11, we determine W_{Br}. The value of 2.8 found from the data compares with a predicted value of 1.8. This discrepancy can be accounted for through an effect called retardation, which reduces the effective Hamaker constant for larger particles (Schenkel and Kitchener, 1960). In any case, we see that the presence of surfactant does not prevent aggregation. As time increases, the formation of larger aggregates (aggregates of more than 10 particles) is favored. However, these tend to be broken up (repeptized) by the particle-counting process.

Shear-induced flocculation in water

For shear-induced flocculation in water, we have used two different volume fractions of particles, 5×10^{-6} and 10^{-5}. As in the Brownian experiment, the particles were diluted into surfactant solution and then mixed with 1.2 M NaCl. After mixing, the sample was transferred to a concentric-cylinder Couette shearing device, the same instrument as that used by Feke and

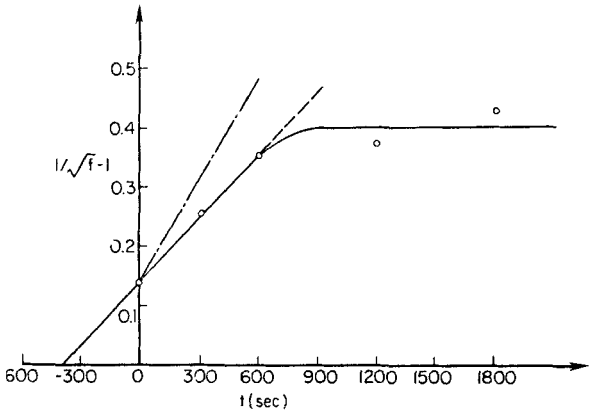

Figure 11. Brownian flocculation in water.

f = fraction of singlets; O, ——— experimental data
From initial slope, $W_{Br} = 2.8$
— · — flocculation rate predicted for unretarded attraction ($W_{Br} = 1.8$) using plot of Feke and Schowalter (1983); backward extrapolation shows the value of an initial "Brownian time"

Schowalter (1985). The outer radius was 6.569 cm, the gap 0.154 cm, and the height 16 cm. A sample size of 150 mL was found to be more than adequate to fill the apparatus. Each sample was sheared at 260 s^{-1} for 10 min. Shearing was stopped periodically to take samples. The samples were immediately diluted to halt coagulation, and particle counting was again used to determine the fractions of singlets.

If we plot $(1/f - 1)$ against time, the theory of shear-induced flocculation indicates that the initial slope will be $8\phi\dot{\gamma}/\pi W_{Sh}$. Here, ϕ is the volume fraction of particles, and W_{Sh} is the stability ratio for flocculation in shear flow. These plots are shown in Figure 12. The experimentally determined stability ratios are 10.3 and 11.1, while a ratio of 5.6 is predicted by Feke and Schowalter (1983). This increase in stability ratio by a factor of 2 is similar to what was found in the Brownian flocculation experiment and again is probably due to retardation. We conclude that the combined effect of retardation and the surfactant layer is to produce a reduction in flocculation rate by approximately a factor of 2, relative to the rate predicted by the theory.

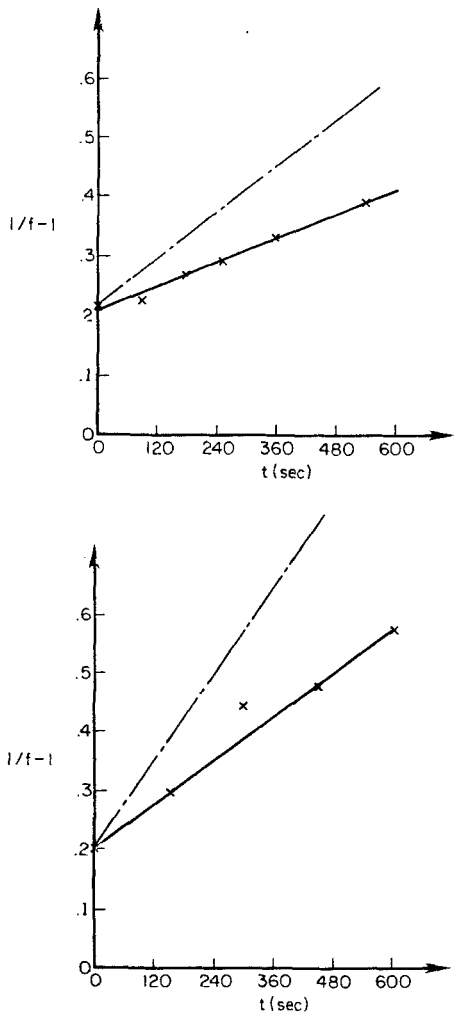

(a) Volume fraction = 5×10^{-6}; $W_{Sh} = 10.3$
(b) Volume fraction = 10^{-5}; $W_{Sh} = 11.1$

Figure 12. Shear-induced flocculation in water.

See text for explanation of ordinate and values of system parameters
X experimentally measured point; ——— a fit to initial rate; — · — expected flocculation rates for unretarded attraction, Eq. 1, $W_{Sh} = 5.6$

Shear-induced flocculation in polymer solutions

The experiments of shear-induced flocculation in polymer solutions were carried out at particle volume fractions of 4×10^{-5} and the polymer concentrations indicated earlier. Base was added to aid in mixing of the polymer solutions. Even with the added base, it took between 3 and 7 min of stirring with a spatula to give the mixture a uniform appearance. Stirring with a spatula instead of a stir bar reduces the shear rate and, therefore, the amount of flocculation induced. It then took from 5 to 7 min to fill the Couette apparatus with the polymer suspension. Procedures were similar to those described earlier, with samples being withdrawn over the course of 10 min of shearing. The MR suspension was sheared at 230 s^{-1}, and the GR at 210 s^{-1}, giving Weissenberg numbers of 15.3 and 10.5, and flow numbers, Fl, of 5.8×10^4 and 1.1×10^5, respectively. We used the value of the viscosity function at the imposed shear rate whenever a viscosity is required for evaluation of a dimensionless group. Viscous heating was unimportant.

After shearing, the samples were diluted into HCl, as described above, to break up any HEC microcrystalline aggregates. When the polymer was sufficiently hydrolyzed, samples were analyzed by particle counting. Results are shown in Figure 13, plotted in the same way as for the shear-in-water experiments. For two of the data points for the MR polymer, the microcrystals were incompletely digested, obscuring most of the particle signal; these data points are indicated by circles.

In Figure 13 the predicted values of $(1/f - 1)$ are shown both with and without the inclusion of a factor of 2 to account for retardation and presence of surfactant. Even with the factor of 2, it is clear that the flocculation rate is much less than that predicted by Newtonian theory.

Experimental Conditions and Their Relation to the Theoretical Results

The experiments of shear-induced flocculation in polymer solutions are consistent with theoretical predictions that the non-Newtonian nature of the suspending fluid can reduce floc-

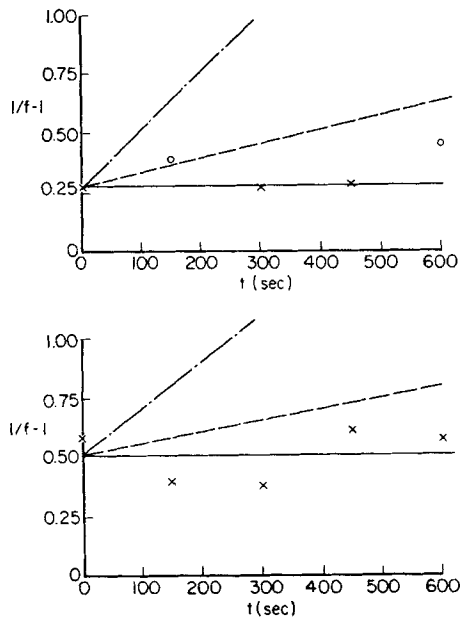

MR HEC, top; GR HEC, bottom

Figure 13. Shear-induced flocculation in polymer solution.

See text for explanation of ordinate and values of system parameters. X experimentally measured point; O particle signal probably obscured by polymer microcrystals, with large error likely; —— best eye-fit to data; — - — Newtonian prediction, Eq. 1; - - - prediction for flocculation rate after influences of retardation and surfactant layer have been factored out

culation rates an order of magnitude below those predicted from a calculation based on Newtonian fluid mechanics.

The experiments were designed to match as closely as possible the conditions used in the calculations. Thus the shear rate was held small enough to maintain the Weissenberg number near a maximum of 10. Relatively large colloidal particles were used for three reasons: to minimize flocculation during mixing with the polymer solution, to minimize the relative thickness of the surfactant layer, and to make small any inhomogeneities in the polymer solution relative to the size of the colloidal particles. The high viscosities of the polymer solutions ensured that Brownian flocculation was not important during the shear-in-polymer experiments.

Polymer solutions were mixed with the particle suspensions by hand in order to reduce the shear rate and therefore the degree of initial flocculation. Even so, it is likely that the mixing caused pockets of relatively high initial degrees of flocculation in local regions of high shear rate. One can probably attribute the scatter of the results of the GR experiment, Figure 13, to such effects since the MR polymer solution required less mixing time.

A further condition on the experiments is that one must be able to detect a clear difference between the flocculation behavior expected in a Newtonian solvent and the actual behavior in a viscoelastic medium. This would suggest that we increase the product $\dot{\gamma}\phi t_t$ to as large a value as possible, where t_t is the total time of shearing. However, a larger ϕ would cause greater initial flocculation, and a larger $\dot{\gamma}$ would take us even farther from the range of We for which calculations are available. Because it was found (Mifflin, 1986) that at high polymer concentrations, such as those used here, polymer eventually begins to displace the surfactant from the particle surfaces, the value of t_t was limited to the range used here.

Unfortunately, the region $0.1 \leq We \leq 1.0$, $\beta = 0.2$, was not accessible with our experimental system. Consequently, although the data we have obtained are consistent with our predictions, further experiments over a range of We are necessary before a cause and effect relation between theory and experiment can be firmly established.

Conclusions

By viewing the results of the theoretical and experimental work as a whole, one can draw certain conclusions about the problem of two spheres interacting in a viscoelastic fluid in particular and the solution of three-dimensional flows of finitely viscoelastic fluids in general.

At $We = 10$ the flocculation rate is substantially reduced by the viscoelastic properties of the suspending fluid.

The GRM method used in our earlier work for a single sphere is a viable alternative to finite element simulations for flows of fluids with finite viscoelasticity around two spherical particles. When only general characteristics of the flow are needed, as is the case here, GRM has a significant edge in computational cost.

Acknowledgment

R. T. Mifflin has been generously supported by the Fannie and John Hertz Foundation. Additional funding has been provided by the Exxon Education Foundation, the Xerox Corporation, and National Science Foundation Grant No. CPE82-12317. The authors would like to thank R. Davis of Hercules, Incorporated, for providing the HEC samples and A. Eidsath for the transmission electron microscopy.

Notation

a = particle radius
A = Hamaker constant
c_i = coefficient in basis function expansion, Eq. 9
E = constant velocity gradient tensor, Eq. 4
f = fraction of particles existing as singlets
Fl = flow number $= 6\pi\mu a^3\dot{\gamma}/A$
$G(t')$ = rate-of-deformation tensor at $t' = \{\nabla v(t') + \nabla v(t')]^T\}/2$
$H = 1 + R^2/2$
i_k = unit vector in the k direction
I = unit tensor
J = rate of disappearance, due to shearing, of singlets per unit volume of suspension
k = Boltzmann's constant
$L(t, t') = R(t, t') \cdot G(t') \cdot R^T(t, t')$
n_0 = initial number density of singlets, Eq. 1
N_1 = primary stress difference, $T_{xx} - T_{yy}$ in notation of Figure 1
p = pressure
q = residual, Eq. 11
r = position vector to a point in space from origin in Figure 1
r_α = position vector to center of sphere α
r = radial coordinate, Figures 3, 4
$R(t, t')$ = rotation tensor, Eq. 8
$R = r/\epsilon^{0.5}$
Re = Reynolds number $= \rho\dot{\gamma}a^2/\mu$
t = time
t_t = total time of shearing
T = absolute temperature
T = extra stress tensor, Eq. 7, with components T_{ij}
v = velocity, with components v_i
v_α = velocity of center of sphere $\alpha(\alpha = 1, 2)$
$v_i(x)$ = basis function, Eq. 9
W = stability ratio, defined by J^o/J
$W(t') = \{\nabla v(t') - [\nabla v(t')]^T\}/2$

We = Weissenberg number = $\lambda_1\dot{\gamma}$, Eq. 7
x = coordinate, Figure 1
x_i = Cartesian coordinate (i = 1, 2, 3)
y = coordinate, Figure 1
z = coordinate, Figure 1
$\tilde{z}$ = coordinate, Figures 3, 4
$Z = \tilde{z}/\epsilon$

Greek letters

$\beta = \lambda_2/\lambda_1$
$\dot{\gamma}$ = shear rate = $\partial v_1/\partial x_2$ for $v = [v_1(x_2), 0, 0]$
$\delta(t)$ = Dirac delta function
ϵ = distance between origin and sphere surface along $\tilde{z}$, Figures 3, 4
ζ = poloidal function, Eq. A4
λ_1 = relaxation time in definition of β, Eq. 7
λ_2 = retardation time in definition of β, Eq. 7
μ = viscosity (in general, shear dependent)
μ_0 = viscosity in the limit of zero shear rate
μ_∞ = viscosity in the limit of infinite shear rate
ρ = density
τ = dimensionless time, $4kTn_0t/3\mu W_{Br}$
ϕ = volume fraction of particles or azimuthal angle in polar coordinate system, Figures 3, 4
ψ = toroidal function, Eq. A3
ω = angular velocity
ω_α = angular velocity of sphere α(α = 1, 2)

Superscripts

o = rate of disappearance of singlets calculated from Smoluchowski's analysis
T = transpose

Subscripts

Br = due to Brownian motion
Sh = due to shear

Appendix: Toroidal and Poloidal Basis Functions

The velocity field used for the toroidal basis function is

$$v_T = \epsilon^{-0.5} R\psi_{,Z}\boldsymbol{i}_\phi - \psi_{,\phi}\boldsymbol{i}_{\tilde{z}}, \tag{A1}$$

and that for the poloidal basis function is

$$v_p = -\epsilon^{-0.5} R\zeta_{,ZZ}\boldsymbol{i}_r + (2\zeta_{,Z} + R\zeta_{,RZ})\boldsymbol{i}_{\tilde{z}} \tag{A2}$$

Commas are used to indicate partial differentiation. Unit vectors refer to the sphere-sphere cylindrical coordinate system shown in Figures 3 and 4. The distance between sphere surfaces along the $\tilde{z}$ axis is 2ϵ, where lengths are scaled in units of a. Also, $Z = \tilde{z}/\epsilon$ and $R = r/\epsilon^{0.5}$. Toroidal and poloidal functions are, respectively,

$$\psi(R, \phi, Z) = \frac{R}{H^6}(Z - H^2)^2 \sin\phi \tag{A3}$$

$$\zeta(R, \phi, Z) = \frac{R}{6H^8}(Z^2 - H^2)^3 \tag{A4}$$

where $H = 1 + R^2/2$ and is, to $0(\epsilon)$, the location of one of the sphere surfaces.

Literature Cited

Battista, O. A., *Microcrystal Polymer Science,* McGraw-Hill, New York (1975).
Bird, R. B., R. C. Armstrong, and O. Hassager, *Dynamics of Polymeric Liquids, I,* Wiley, New York (1977).
Bush, M. B., J. F. Milthorpe, and R. I. Tanner, "Finite Element and Boundary Element Methods for Extrusion Calculations," *J. Non-Newtonian Fluid Mech.*, **16,** 37 (1984).
Chandrasekhar, S., *Hydrodynamic and Hydromagnetic Stability,* Clarendon, Oxford, (1961).
Cox, R. G., "The Motion of Suspended Particles Almost in Contact," *Int. J. Multiphase Flow,* **1,** 343 (1974).
Feke, D. L., and W. R. Schowalter, "The Effect of Brownian Diffusion on Shear-Induced Coagulation of Colloidal Dispersions," *J. Fluid Mech.*, **133,** 17 (1983).
———, "The Influence of Brownian Diffusion on Binary Flow-Induced Collision Rates in Colloidal Dispersions," *J. Coll. Interface Sci.*, **106,** 203 (1985).
Goodwin, J. W., R. H. Ottewill, R. Pelton, G. Vianello, and D. E. Yates, "Control of Particle Size in the Formation of Polymer Latices," *British Pol. J.*, **10,** 173 (1976).
Graessley, W. W., "The Entanglement Concept in Polymer Rheology," *Adv. Pol. Sci.*, **16,** 1 (1974).
Hunter, R. J., *Zeta Potential in Colloid Science: Principles and Applications,* Academic Press, New York. (1981).
Israelachvili, J. N., *Intermolecular and Surface Forces: With Applications to Colloidal and Biological Systems,* Academic Press, New York (1985).
Mahanty, J., and B. W. Ninham, *Dispersion Forces,* Academic Press, New York (1976).
Mifflin, R. T., "Kinetics of the Flocculation of Colloids in Viscoelastic Media under Shear," Ph.D. Diss., Princeton Univ. (1986).
Mifflin, R. T., and W. R. Schowalter, "A Numerical Technique for Three-Dimensional Steady Flows of Fluids of the Memory-Integral Type," *J. Non-Newtonian Fluid Mech.*, **20,** 323 (1986).
Napper, D. H., *Polymeric Stabilization of Colloidal Dispersions,* Academic Press, New York (1983).
Peery, J. H., "Fluid Mechanics of Rigid and Deformable Particles in Shear Flow at Low Reynolds Numbers," Ph.D. Diss. Princeton Univ. (1966).
Russel, W. B., "Brownian Motion of Small Particles Suspended in Liquids," *Ann. Rev. Fluid Mech.*, **13,** 425, M. Van Dyke, J. V. Wehausen, J. L. Lumley, eds., Annual Reviews Inc., Palo Alto (1981).
Schenkel, J. H., and J. A. Kitchener, "A Test of the Derjaguin-Verwey-Overbeek Theory with a Colloidal Suspension," *Trans. Faraday Soc.*, **56,** 161 (1960).
Schowalter, W. R., *Mechanics of Non-Newtonian Fluids,* Pergamon, New York (1978).
———, "Stability and Coagulation of Colloids in Shear Fields," *Ann. Rev. Fluid Mech.*, **16,** 245, M. Van Dyke, J. V. Wehausen, J. L. Lumley, eds., Annual Reviews Inc., Palo Alto (1984).
Sperry, P. R., H. B. Hopfenberg, and N. L. Thomas, "Flocculation of Latex by Water-Soluble Polymers: Experimental Confirmation of a Nonbridging, Nonabsorptive, Volume-Restriction Mechanism," *J. Coll. Interface Sci.*, **82,** 62 (1981).
Tiefenbruck, G., and L. G. Leal, "A Numerical Study of the Motion of a Viscoelastic Fluid Past Rigid Spheres and Spherical Bubbles," *J. Non-Newtonian Fluid Mech.*, **10,** 115 (1982).
Van de Ven, T. G. M., and S. G. Mason, "The Microrheology of Colloidal Dispersions. IV: Pairs of Interacting Spheres in Shear Flow," *J. Coll. Interface Sci.*, **57,** 505 (1976).
Zeichner, G. R., and W. R. Schowalter, "Effects of Hydrodynamic and Colloidal Forces on the Coagulation of Dispersions," *J. Coll. Interface Sci.*, **71,** 237 (1979).

Manuscript received July 16, 1987, and revision received June 7, 1988.